Effect of the Preparation Method on the Electrocatalytic Activity of Pt-Sn/Nanotubes Catalysts Used in DMFC

Virginia I. Rodríguez,[z] Natalia S. Veizaga, and Sergio R. de Miguel

Instituto de Investigaciones en Catálisis y Petroquímica "Ing. José Miguel Parera" (INCAPE), Facultad de Ingeniería Química (UNL)-CONICET, 3000 Santa Fe, Argentina

A series of bimetallic Pt-Sn catalysts supported on multiwalled carbon nanotubes (NT) for methanol oxidation reaction was prepared by different methods that involve ethylene glycol synthesis under reflux conditions and sodium borohydride reduction (using water or ethylene glycol as solvents) at 55°C. Pt-Sn/NT catalysts containing 20 wt% platinum with Pt:Sn atomic ratios of 5:1, 3:1 and 1:1 were prepared and their morphology and electrocatalytic activities were characterized by temperature programmed reduction, X-ray photoelectron spectroscopy, H_2 chemisorption, benzene hydrogenation reaction, transmission electron microscopy, cyclic voltammetry, linear sweep voltammetry, chronoamperometry and CO stripping. The electrocatalysts performance depends strongly on the preparation method and Pt:Sn atomic ratios, with the Pt_3Sn_1/NT sample prepared by ethylene glycol displaying the highest activity for methanol electrooxidation, a good CO tolerance and an important stability.
© 2017 The Electrochemical Society. [DOI: 10.1149/2.1811713jes] All rights reserved.

Direct alcohol fuel cells are considered very attractive energy systems because of their high conversion efficiency, high energy density, adaptability to portable devices, low temperature operation and employment of an easily handled reactant as alternative to hydrogen. Low-weight molecular alcohols such as methanol and ethanol can be used, leading to direct methanol (DMFC) and ethanol fuel cells (DEFC).[1,2]

A Pt/C electrocatalyst is one of the best materials to be used in low-temperature fuel cells. However, Pt is expensive and it is not the best catalyst for anode material owing to vulnerability toward poisoning by CO or carbonaceous intermediates. Alcohol oxidation on a Pt/C catalyst takes place with the formation of adsorbed CO as intermediate, which becomes a poison on the active sites and significantly reduces the cell performance.[3] To produce a useful electrocatalyst, significant efforts have been made to decrease the amount of Pt used and to overcome the problem of CO poisoning.[4–8] The solutions involve the use of secondary metals such as Ru,[9–11] Sn,[10,12–14] Pd,[11,12] Mo,[15,16] W,[17,18] Rh[6,19,20] and Cr[21,22] to promote the catalytic activity and the oxidation of the chemisorbed CO. Recently, utilization of PtSn over different carbonaceous materials as anode catalysts has been studied for methanol oxidation by several groups.[14,23–27]

Different methodologies for the synthesis of metal nanoparticles supported on high surface area carbons play a key role to attain materials with homogeneous metallic distribution, small particle size and high catalytic activity. Thus, several methods for the synthesis of PtSn/C catalysts have been developed: conventional impregnation,[28,29] polyol method,[22,30–32] microwave-assisted heating,[33,34] thermal decomposition of polymeric precursors method[35–38] and borohydride reduction.[39,40]

In polyol method, the reflux of an ethylene glycol solution provides homogeneous dispersions of the corresponding metal nanoparticles. The alcohol simultaneously acts as solvent and reducing agent. This method offers some advantages such as good reproducibility, satisfactory distribution and small particle size. Also, dispersed platinum-based catalysts supported on carbon have been obtained by sodium borohydride reduction. In this methodology, catalysts are formed by addition of high surface area carbon support to a sodium borohydride solution, enabling good control of nanoparticle size and composition.

In this context, the aim of this work is to carry out a systematic study of Pt-Sn nanoparticles supported on multiwalled carbon nanotubes with Pt:Sn atomic ratios of 5:1, 3:1 and 1:1 and to compare the nanoparticles obtained by chemical reduction with sodium borohydride and ethylene glycol, in terms of morphology and electrocatalytic activity for methanol oxidation, with these obtained by more conventional methods.

The supported metallic phases were characterized by temperature programmed reduction, X-ray photoelectron spectroscopy, H_2 chemisorption, benzene hydrogenation reaction, transmission electron microscopy, cyclic voltammetry, linear sweep voltammetry, chronoamperometry and CO stripping.

Experimental

Catalyst preparation.—Commercial multiwalled carbon nanotubes (NT) from Sunnano (purity > 90%, diameter: 10–30 nm, length: 1–10 μm) with the following textural properties: $S_{BET} = 211$ m^2 g^{-1} and $V_{pore} = 0.46$ cm^3 g^{-1} were used as carbonaceous support. The metallic precursors were $H_2PtCl_6.6H_2O$ (Tetrahedron) and $SnCl_2.2H_2O$ (Cicarelli). Sodium borohydride (Merck) and ethylene glycol (Merck) were the reducing agents.

Before the synthesis, multiwalled carbon nanotubes were purified in order to remove all inorganic impurities. The purification consisted on successive treatments with 10 wt% HCl, HNO_3 and HF aqueous solutions at room temperature for 48 h without stirring. After HCl and HNO_3 treatments, NT were washed until pH = 4. After HF treatment, NT were washed until deionized water pH. Then, NT were filtered and dried in an oven at 120°C for 24 h. Finally, the powder was heated to 800°C under H_2 atmosphere for 4 h to eliminate sulfurated traces that could poison the metallic phase.[41,42]

In the polyol method[19,43] carbon nanotubes were dispersed in a mixture solution of water:ethylene glycol (1:3 in volume ratio) and ultrasonicated for 30 min. Then, the corresponding quantities of precursors of Pt and Sn were added to the carbon slurry. After being kept under reflux for 2 h, the mixture was filtered, washed with copious deionized water and dried at 70°C for 2 h in a vacuum oven. These samples are denoted as Pt-Sn/NT (EG).

For sodium borohydride reduction method,[40,44] carbon nanotubes were dispersed into water and stirred for 30 min at 55°C. Then, calculated amounts of H_2PtCl_6 and $SnCl_2$ solutions were added to the above mixture and stirred for 30 min. A freshly prepared 0.4 M $NaBH_4$ solution (in 1 M NaOH) was added drop by drop into the above solution under vigorous stirring. After stirring for 1 h, the obtained mixture was cooled up to room temperature, filtered and washed repeatedly with deionized water. The formed powder was dried at 70°C for 2 h in a vacuum oven. The catalysts are denoted as Pt-Sn/NT ($NaBH_4$).

For sodium borohydride reduction method in ethylene glycol,[45] the support was dispersed into EG (instead of water) and the same procedure as that above described was employed. The catalysts are denoted as Pt-Sn/NT ($NaBH_4$-EG).

For the sake of comparison, monometallic Pt/NT catalysts were also prepared. The nominal loading of Pt in all catalysts was 20 wt%. Table I summarizes nominal Sn loadings for the bimetallic catalysts.

[z]E-mail: virodri@fiq.unl.edu.ar

Table I. Nominal metal loading, Pt:Sn atomic ratios and hydrogen chemisorption values (H) of Pt/NT and Pt-Sn/NT catalysts.

Catalyst	Nominal Metal Loading [wt%]		Nominal Pt:Sn atomic ratio	H [μmol H$_2$ g cat^{-1}]
	Pt	Sn		
Polyol Method				
Pt/NT (EG)	20			308
Pt$_5$Sn$_1$/NT (EG)	20	2.43	5:1	311
Pt$_3$Sn$_1$/NT (EG)	20	4.06	3:1	318
Pt$_1$Sn$_1$/NT (EG)	20	12.17	1:1	348
Sodium Borohydride Reduction Method				
Pt/NT (NaBH$_4$)	20			74
Pt$_5$Sn$_1$/NT (NaBH$_4$)	20	2.43	5:1	150
Pt$_3$Sn$_1$/NT (NaBH$_4$)	20	4.06	3:1	156
Pt$_1$Sn$_1$/NT (NaBH$_4$)	20	12.17	1:1	117
Sodium Borohydride Reduction Method (in EG)				
Pt/NT (NaBH$_4$-EG)	20			150
Pt$_5$Sn$_1$/NT (NaBH$_4$-EG)	20	2.43	5:1	258
Pt$_3$Sn$_1$/NT (NaBH$_4$-EG)	20	4.06	3:1	257
Pt$_1$Sn$_1$/NT (NaBH$_4$-EG)	20	12.17	1:1	276

Catalyst characterizations.—*Structural analysis.*—*Temperature programmed reduction (TPR).*—After metal deposition, catalysts were reduced by using a reductive mixture (10 mL min^{-1} of H$_2$ (5%vol)-N$_2$) in a flow reactor. Samples were heated at 6°C min^{-1} from 25 to 800°C. The exit of the reactor was connected to a thermal conductivity detector in order to obtain the TPR signal.

X-Ray photoelectron spectroscopy (XPS).—XPS measurements were carried out in a Multitechnic Specs Photoemission Electron Spectrometer equipped with an X-ray source Mg/Al and a hemispherical analyzer PHOIBOS 150 in the fixed analyzer transmission (FAT) mode. The spectrometer operates with an energy power of 100 eV and the spectra were obtained with a pass energy of 30 eV and a Mg anode operated at 90 W. The analysis chamber was kept at pressure lower than 1.5×10^{-8} torr. The binding energies (BEs) of the signals were referred to the C1s peak at 284 eV. Peak areas values were estimated by fitting the signals with a combination of Lorentzian–Gaussian curves of variable proportion and using the CasaXPS Peak fit software version 1.

H$_2$ chemisorption.—H$_2$ chemisorption measurements were made in a volumetric equipment at room temperature. The sample was previously outgassed under vacuum (10^{-4} Torr) at 100°C for 30 min. The H$_2$ adsorption isotherms were obtained between 25 and 100 Torr. The isotherms were linear in the range of used pressures and the H$_2$ chemisorption capacities were calculated by extrapolation of the isotherms to zero pressure.

Benzene hydrogenation reaction.—The benzene (Bz) hydrogenation reaction was carried out in a differential flow reactor at 110°C with a H$_2$/Bz molar ratio equal to 26 and a volumetric rate of 600 mL min^{-1}. The activation energy in benzene hydrogenation (Ea$_{Bz}$) was obtained by measuring the initial reaction rate at 110, 100 and 90°C. The reaction products were analyzed by a gas chromatographic system (packed column with Chromosorb and FID as detector).

Electrochemical measurements.—All electrochemical measurements were performed on a potentiostat/galvanostat (TEQ–02, Argentina) and a three electrode test cell at 30°C. The working electrode was a thin layer of Nafion impregnated Pt-Sn/NT composite cast on a vitreous carbon disk electrode. The counter electrode was a Pt wire and the reference electrode was an Ag/AgCl electrode. 10 mg catalyst was suspended in a mixture of 160 μL of isopropanol and 80 μL of Nafion solution. This mixture was ultrasonically scattered for 35 min to form a homogeneous ink and 8 μL of this ink was then placed on the vitreous electrode with a 5 mm diameter to act as the working electrode. Ultra pure N$_2$ was passed through the cell for 10 min to remove oxygen from the electrolyte solution before measurements. A N$_2$ atmosphere was maintained above the solution during the experiments.

CO stripping.—Pure CO was bubbled in an electrolytic solution of 0.5 M H$_2$SO$_4$. During the CO adsorption process (60 min), the potential of the cell was kept constant at 200 mV vs Ag/AgCl. Then, N$_2$ was passed to purge the electrolytic solution in order to eliminate the dissolved CO, thus remaining only the adsorbed CO on the Pt surface. Under these conditions, and maintaining constant the flow of inert gas, the potential was modified in order to induce the CO oxidation. The electrochemical active surface (EAS) -Eq. 1- was obtained from the CO voltammetry as:

$$EAS = \frac{(Q_{CO}/q_{CO}^s)}{m_{Pt}} \quad [1]$$

where m_{Pt} is the Pt mass, Q_{CO} is the charge required for the oxidation of the monolayer of CO adsorbed on the active sites, and q^s_{CO} is a reference value equal to 0.42 mC cm^{-2} (assuming that the surface density of polycrystalline Pt is 1.3×10^{15} atoms cm^{-2}), and that each CO molecule is adsorbed on a single Pt atom, and two electrons are involved in the oxidation of CO to CO$_2$.[46]

Cyclic voltammetry (CV).—The electrochemical activities of the catalysts toward methanol oxidation were carried out in a 0.5 M H$_2$SO$_4$ + 1 M CH$_3$OH solution. The scan range was from −200 to 1200 mV vs Ag/AgCl and the scan rate was 25 mV s^{-1}.

Linear sweep voltammetry (LSV).—Linear sweep voltammetry was carried out in a deaerated 0.5 M H$_2$SO$_4$ + 1 M CH$_3$OH solution at a scan rate of 1 mV s^{-1} to evaluate the catalyst activity for methanol oxidation.

Chronoamperometric measurements.—The tests were carried out to evaluate the effect of the electrode potential on methanol oxidation in solution of 0.5 M H$_2$SO$_4$ + 1 M CH$_3$OH for 60 min. The potential was fixed at 350 mV vs Ag/AgCl.

Results and Discussion

Figure 1 shows temperature programmed reduction (TPR) profiles of Pt and Pt-Sn catalysts supported on NT and prepared by different deposition-reduction techniques in liquid phase (polyol, sodium borohydride and sodium borohydride in ethylene glycol methods). For comparative purposes, TPR profiles of Pt/NT and Pt-Sn/NT catalysts prepared by conventional impregnation (CI)[47] are also included (Fig. 1a). Besides, TPR profiles of Sn(12.17 wt%)/NT (CI) and Sn(12.17 wt%)/NT (EG) and the profile corresponding to purified nanotubes are also included.

Pt catalysts prepared by conventional impregnation (Fig. 1a) exhibit a large peak at about 180–200°C corresponding to the reduction of oxychloroplatinum species.[48] It can be observed that this maximum is shifted to lower values for bimetallic Pt-Sn catalysts. The TPR
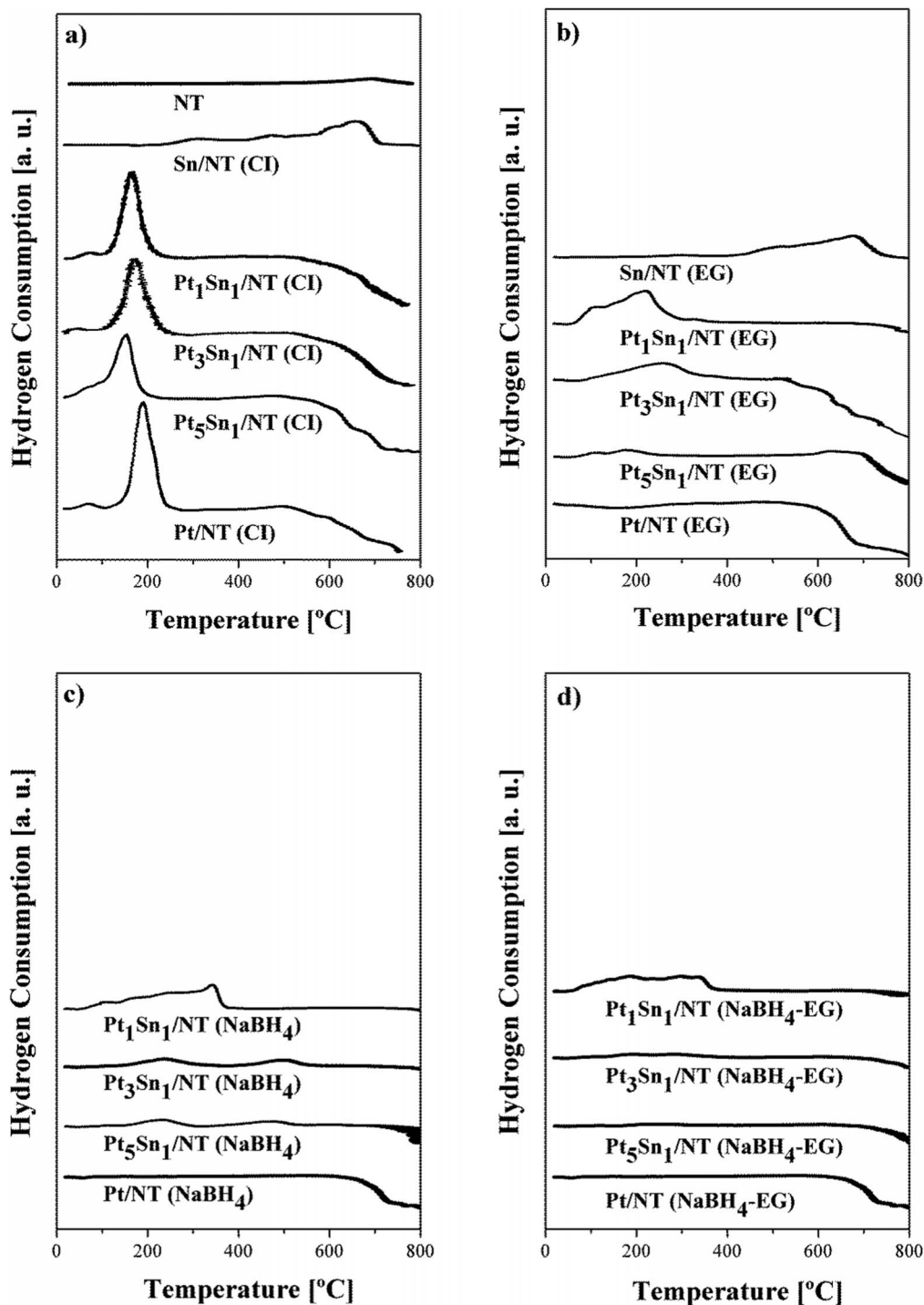
Figure 1. TPR profiles of Pt/NT and Pt-Sn/NT catalysts prepared by: a) CI; b) EG; c) NaBH$_4$; and d) NaBH$_4$-EG methods.

profile of Sn(12.17 wt%)/NT (CI) shows that Sn species are reduced at high temperature; however this signal does not appear in bimetallic Pt-Sn samples prepared by conventional impregnation. This fact suggests that the presence of reduced Pt near Sn species would catalyze the reduction of a fraction of the promoter at lower temperatures, in the zone of Pt reduction.

It is important to note that TPR profiles of Pt-Sn/NT catalysts (with higher Pt/Sn ratios) prepared by EG (Fig. 1b), NaBH$_4$ (Fig. 1c) and NaBH$_4$-EG (Fig. 1d) show very small reduction peaks in the Pt zone where Pt is reduced in the conventionally impregnated catalysts (Fig. 1a). This would indicate that the major fraction of Pt would be

in metallic state (Pt^0) at the end of the deposition-reduction method. However, TPR profiles of Pt-Sn catalysts prepared by EG, NaBH$_4$ and NaBH$_4$-EG, with a Pt/Sn molar ratio equal to 1, show wider reduction zones appearing up to 400°C, which could be attributed to the reduction of tin species by a spillover effect promoted by the presence of reduced platinum.

The very small peaks located around 500°C for Pt$_3$Sn$_1$/NT (NaBH$_4$) and Pt$_5$Sn$_1$/NT (NaBH$_4$) (Fig. 1c) could be due to the reduction of Sn^{2+} and Sn^{4+} species.[39]

In order to find more information about the Pt and Sn reducibilities of the bimetallic catalysts supported on NT, a XPS characterization
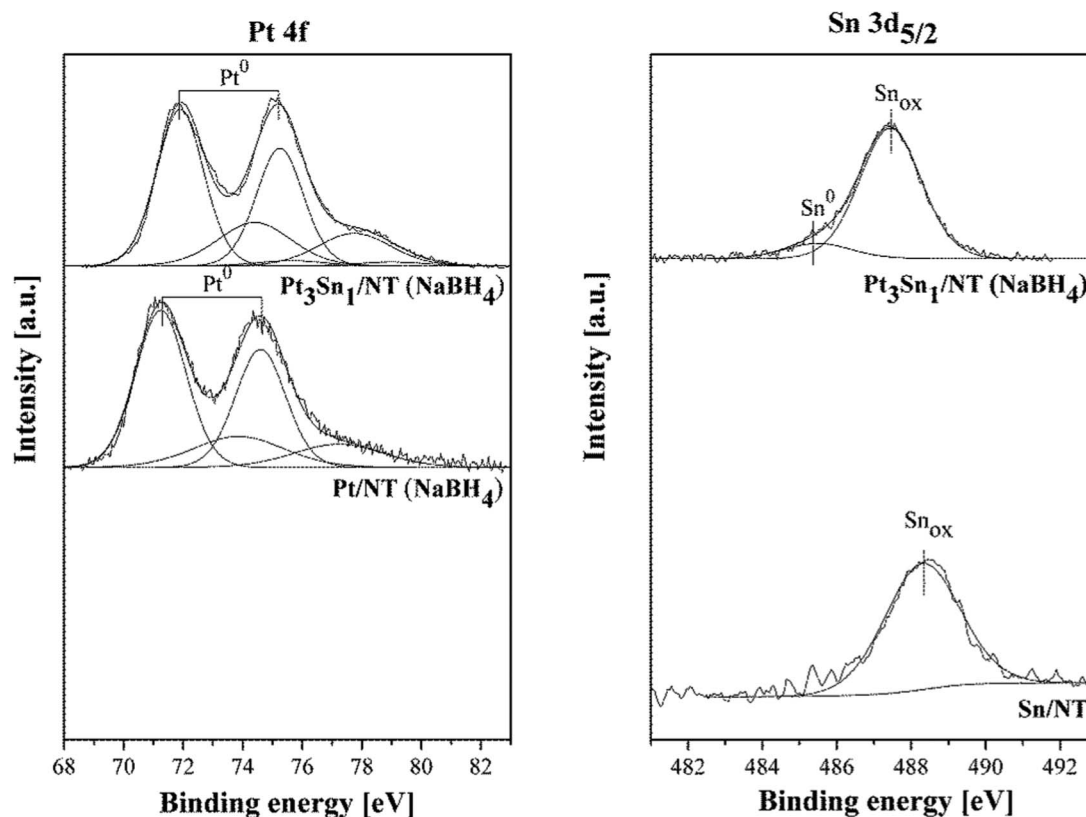
Figure 2. Pt 4f and Sn 3d XPS signals of Pt_3Sn_1/NT, Pt/NT and Sn/NT catalysts prepared by $NaBH_4$ method.

of the Pt/NT, Pt_3Sn_1/NT and Sn/NT catalysts prepared by $NaBH_4$ method was done as Figure 2 shows. For the monometallic catalyst (Pt/NT), the Pt 4f signal was deconvoluted and one peak at 71.2 eV was obtained for Pt $4f_{7/2}$ and other one at 74.6 eV for Pt $4f_{5/2}$. These peaks are assigned to zerovalent Pt.[49] However, other small doublets at 73.7 eV and 76.3 eV corresponding to Pt oxides or oxychlorides are also present. The concentrations of oxidized surface species are 35%, hence an important amount of Pt is in the zerovalent state (65%).

From the deconvolution of Pt 4f spectra in the bimetallic Pt_3Sn_1/NT catalyst, a peak at 71.8 eV was obtained for the Pt $4f_{7/2}$ signal and another peak at 75.0 eV for Pt $4f_{5/2}$. These peaks correspond to the zerovalent state of Pt. Two additional small doublets are also observed in Figure 2, one at 74.3 eV and 77.8 eV and the other one at 75.5 eV and 78.4 eV, these corresponding to oxides or oxychlorides of Pt. The concentration of the surface oxidized species was lower than 35%, this meaning that most of surface Pt species (>65%) are in metallic state. It is noteworthy that in Pt_3Sn_1/NT catalyst the binding energy shifts to higher values compared to Pt/NT catalyst, which may be caused by an electronic modification of the Pt centers due to the presence of the promoter (Sn).

XPS of Sn 3d of Pt_3Sn_1/NT catalyst shows that Sn forms oxidized species and a small proportion of zerovalent Sn (about 15%) was found. However, the XPS signal corresponding to the monometallic Sn/NT catalyst displays only oxidized tin species. Hence, there is a catalytic effect of Pt on the Sn reduction, and the small fraction of metallic tin could be probably forming alloys with metallic Pt.

Hydrogen chemisorption values of Pt and Pt-Sn catalyst series are shown in Table I. Bimetallic catalysts supported on NT and prepared by EG showed H_2 chemisorption values slightly higher than the corresponding monometallic one, while Pt-Sn/NT ($NaBH_4$) and Pt-Sn/NT ($NaBH_4$-EG) catalysts presented H_2 chemisorption values much higher than the corresponding Pt/NT ones. The increase of these values for bimetallic samples (respect to the corresponding monometallic ones) could be due either to a decrease of the particle

size or to the presence of geometric/electronic effects of the promoter on Pt sites.

Table II shows the results of initial reaction rates and activation energies in benzene hydrogenation for mono- and bimetallic catalysts prepared by EG, $NaBH_4$ and $NaBH_4$-EG. Considering that the benzene hydrogenation is a structure-insensitive reaction, changes in activation energy (Ea_{Bz}) can be related to electronic modifications of the active sites.[50,51] This test reaction of the metallic phase can be used to characterize catalysts prepared by deposition-reduction in

Table II. Initial reaction rate (R_{Bz}^0) and activation energy (Ea_{Bz}) in benzene hydrogenation reaction for Pt/NT and Pt-Sn/NT catalysts.

Catalyst	R_{Bz}^0 [mol h^{-1} g Pt^{-1}]	Ea_{Bz} [Kcal mol^{-1}]
Polyol Method		
Pt/NT (EG)	2.33	7.88
Pt_5Sn_1/NT (EG)	0.43	10.53
Pt_3Sn_1/NT (EG)	0.75	11.43
Pt_1Sn_1/NT (EG)	n.d.	n.d.
Sodium Borohydride Reduction Method		
Pt/NT ($NaBH_4$)	2.75	10.89
Pt_5Sn_1/NT ($NaBH_4$)	0.42	16.17
Pt_3Sn_1/NT ($NaBH_4$)	0.50	13.45
Pt_1Sn_1/NT ($NaBH_4$)	n.d.	n.d.
Sodium Borohydride Reduction Method (in EG)		
Pt/NT ($NaBH_4$-EG)	1.93	12.14
Pt_5Sn_1/NT ($NaBH_4$-EG)	1.30	12.45
Pt_3Sn_1/NT ($NaBH_4$-EG)	0.29	13.64
Pt_1Sn_1/NT ($NaBH_4$-EG)	n.d.	n.d.

n.d.: not determined due to the low activity of the sample.
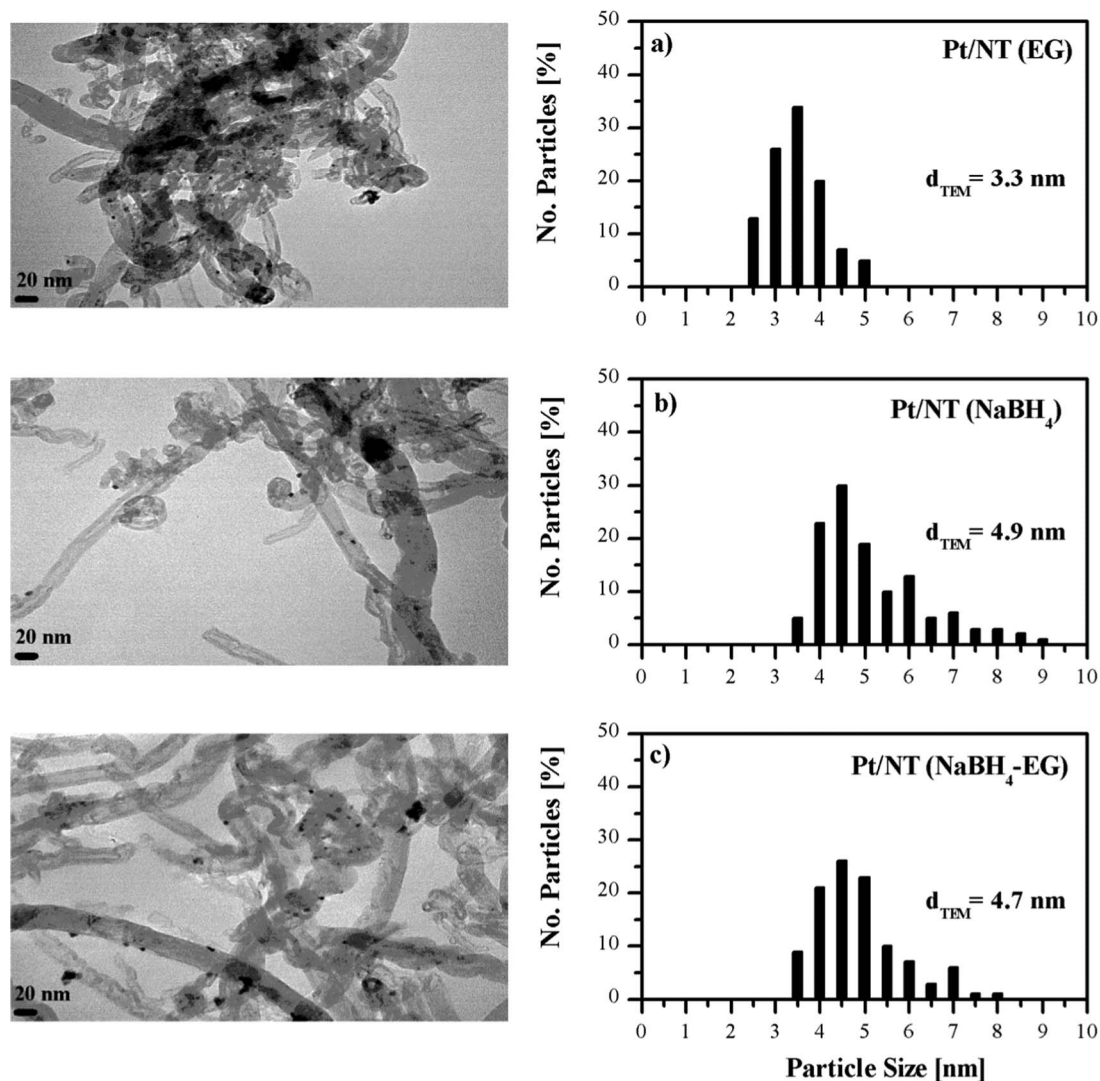
Figure 3. TEM images and particle size distributions of Pt/NT catalysts prepared by: a) EG; b) NaBH₄; and c) NaBH₄-EG methods.

liquid phase at low temperature, since the temperature used for this reaction is also low (100–130°C) so changes in the characteristics of the catalysts by the temperature would be avoided. The activation energy values of the bimetallic catalysts prepared by EG, NaBH₄ and NaBH₄-EG are higher than those of the corresponding monometallic ones. This indicates electronic effects of the promoter on the active sites of Pt with probable alloys formation. The drastic decrease of the initial activities of the bimetallic catalysts with the increase of the Sn content would be due not only to the presence of these electronic effects but also to additional geometric ones, mainly blocking.

The distribution of particle sizes of Pt/NT and Pt_3Sn_1/NT electrocatalysts were examined by transmission electron microscopy (TEM). For each catalyst, a microphotography, the distribution and mean values of the particle sizes are displayed in Figures 3 and 4. TEM results indicate that Pt/NT catalyst prepared by deposition-reduction with EG has a mean particle size lower than the ones prepared by NaBH₄ and NaBH₄-EG methods. In this sense, the polyol method would assure a stronger interaction between the support and the metallic precursor during the deposition-reduction in liquid phase, leading to higher dispersions of the metallic phase in agreement with chemisorption values (see Table I). Furthermore, the formation of NaBH₄–EG reaction complex, which is both a reducing agent and a stabilizer, may also influence the particle morphology (Fig. 3).[52]

In the case of bimetallic catalysts prepared by the polyol method, there is a slight modification of the mean particle size (Fig. 4) that correlates well with chemisorption measurements (Table I). On the other hand, Sn addition to Pt by the other deposition-reduction methods (NaBH₄ and NaBH₄-EG) produces an important decrease of the mean particle size (from 4.9 to 3.6 nm and from 4.7 to 3.2 nm, respectively), in agreement with the important increase of the chemisorption values of bimetallic catalysts with respect to the corresponding monometallic ones.

Figure 5 shows the cyclic voltammograms of CO stripping corresponding to mono- and bimetallic catalysts. Pt/NT (EG) catalyst shows a narrow CO oxidation peak at about 600 mV vs Ag/AgCl, this value being similar to the one found by Vidakovic et al.[53] who reported 536 mV vs Ag/AgCl for the CO stripping potential peak of a commercial unsupported Pt catalyst. For Pt/NT prepared by NaBH₄ and NaBH₄-EG, the CO oxidation peaks appear at about 600 and 500 mV vs Ag/AgCl, respectively.

For some bimetallic electrocatalysts supported on NT, the CO oxidation peak is divided, thus appearing a main and wide peak at 500 mV and a small one at 200 mV vs Ag/AgCl. The first peak would correspond to the oxidation of weakly adsorbed CO on metallic sites, while the second one would be due to the oxidation of strongly adsorbed CO on other Pt sites modified by the closeness of the second
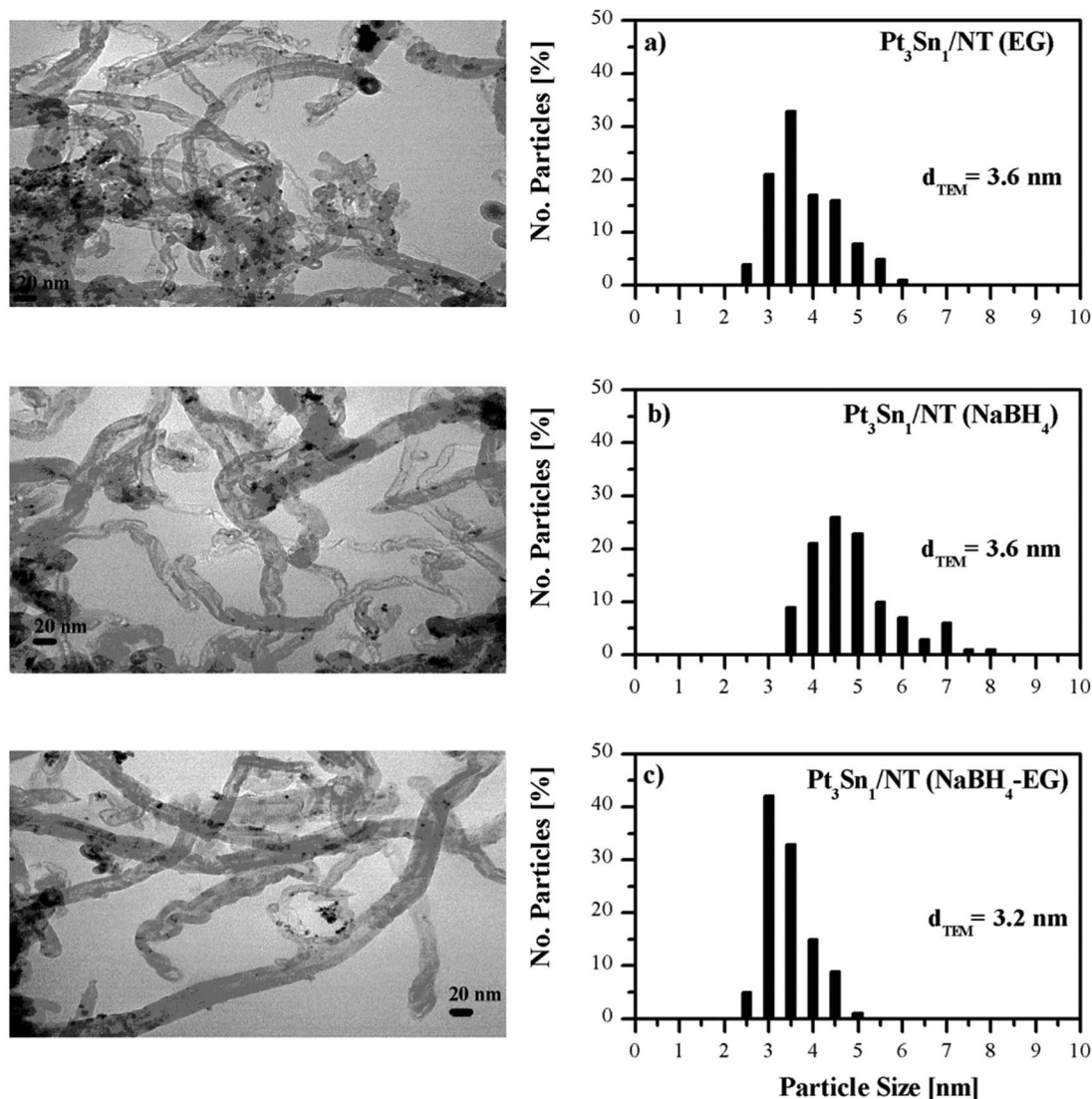
Figure 4. TEM images and particle size distributions of Pt_3Sn_1/NT catalysts prepared by: a) EG; b) $NaBH_4$; and c) $NaBH_4$-EG methods.

metal (Sn). Similar effects were observed for supported PtIn and PtGe electrocatalysts.[54]

Table III shows the onset potential of CO oxidation and electrochemical active surfaces (EAS) of bimetallic catalysts compared with those of the corresponding monometallic ones. It is clearly observed that the beginning of the CO oxidation is shifted to much lower potentials for all Pt-Sn catalysts.

For the monometallic Pt catalysts, the onset potentials are found at 365 mV vs Ag/AgCl for Pt/NT (EG), 479 mV vs Ag/AgCl for Pt/NT ($NaBH_4$) and 300 mV vs Ag/AgCl for Pt/NT ($NaBH_4$-EG), whereas that of the corresponding bimetallic ones are placed at much lower values, between 111 and 172 mV vs Ag/AgCl. It is clearly evidenced an important promoting effect of Sn, which promotes the CO oxidation at lower potentials, this improving the CO tolerance of the anodic electrocatalyst.

The earlier oxidation of CO_{ads} in Sn containing electrodes, compared with the corresponding Pt one, could be explained not only by the Sn ability to adsorb OH at more negative potentials than Pt but by the reactions of surrounding CO_{ads} species over Pt sites (bifunctional mechanism) or the modification of the d electronic Pt bands by Sn as well.[55] In this sense, characterization and CO stripping results would be indicating that there exist promoting effects of Sn over Pt in catalysts supported on NT. This could be explained by the presence of electronic and geometric modifications caused by the promoter placed

in the vicinity of the active metallic phase. These promoting effects would ease the oxidation of CO to CO_2 at lower potentials than in the case of monometallic catalysts.

As it can be seen, NT supported monometallic catalysts prepared by EG give high EAS values (Table III), bimetallic ones showing an increase respect to them in agreement with chemisorption results.

Considering the important promoting effect of Sn, which improves the CO tolerance of the anodic electrocatalyst, the activities of Pt/NT and Pt-Sn/NT catalysts prepared by EG, $NaBH_4$ and $NaBH_4$-EG were examined by cyclic voltammetry technique (CV) for the oxidation reaction of methanol (MOR). In order to obtain the voltammograms of H_2 adsorption/desorption (Fig. 6), the potential was cycled between −200 and 1200 mV vs Ag/AgCl at 25 mV s^{-1} in a nitrogen-purged 0.5 M H_2SO_4 + 1 M CH_3OH electrolyte solution at 30°C. The 5th cycle from all CV curves was selected in order to obtain a reproducible and reliable electrocatalytic performance in the half cell reaction. The shapes of the curves are typical for the oxidation reactions of simple organic alcohols, showing two anodic current peaks in positive and negative sweeps, respectively. They are related to oxidation reactions of alcohol in the positive sweep and to incompletely oxidized carbonaceous residues on the catalyst surface during the negative sweep. Table IV shows the CV results of the different catalysts for methanol oxidation reaction.
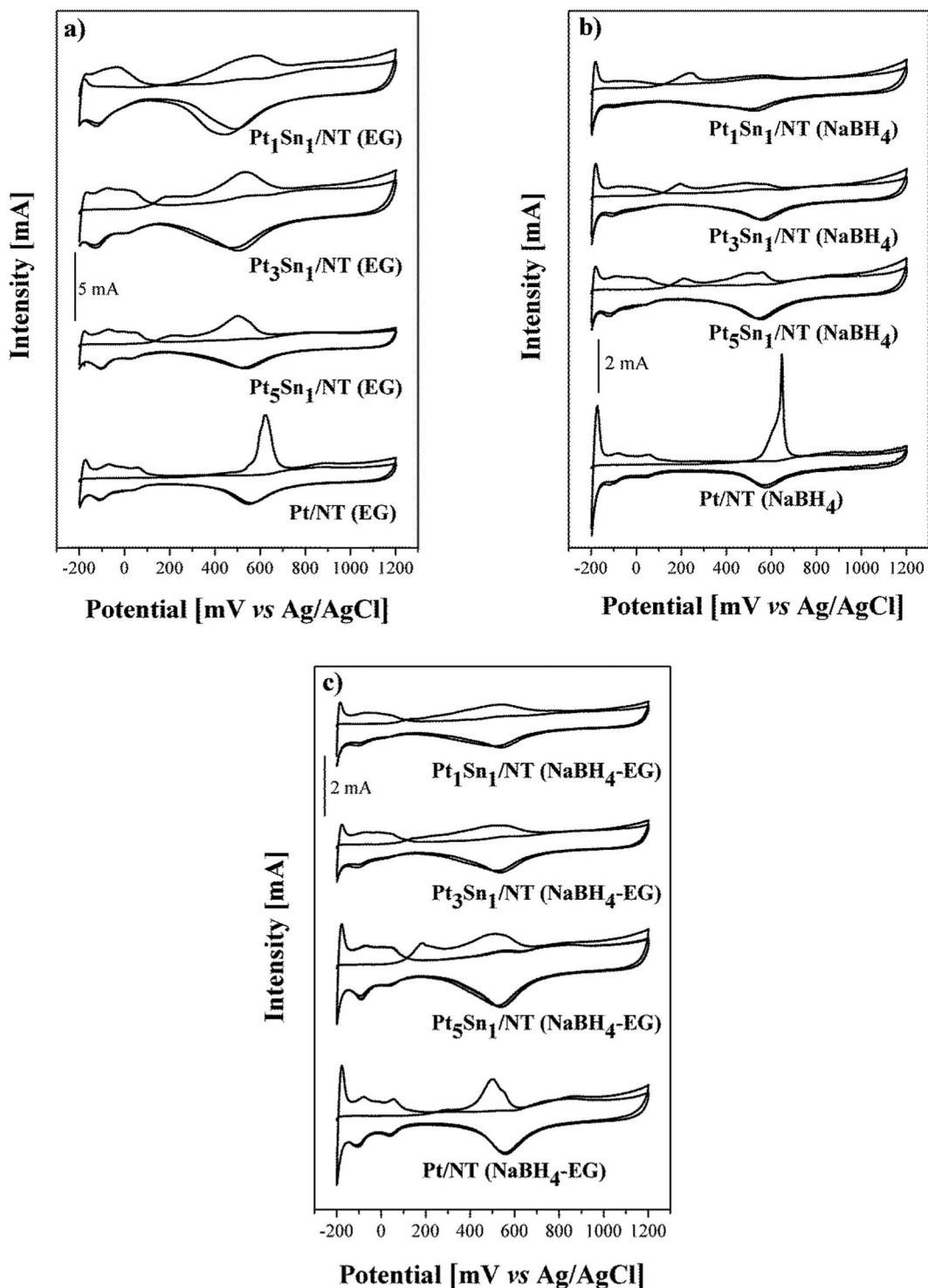
Figure 5. Cyclic CO stripping voltammograms for Pt/NT and Pt-Sn/NT catalysts prepared by: a) EG; b) NaBH$_4$; and c) NaBH$_4$-EG methods. Electrolytic solution: 0.5 M H$_2$SO$_4$.

By comparing the positive peak current obtained for the methanol oxidation of the different bimetallic and monometallic catalysts prepared by the three techniques (Table IV), it is clear that tin participates as a promoter to increase the electrocatalytic performance of Pt. In addition, the increase of the Sn addition to Pt (from 2.43 wt% to 4.06 wt%) leads to substantial enhancements in the catalytic activity for the methanol oxidation, mainly for catalysts prepared by EG and NaBH$_4$. However, for the bimetallic catalysts with the highest Sn content (12.17 wt%), the activities decrease. Hence, there is an optimum

in the catalytic activity for the three Pt-Sn catalysts prepared with a Pt:Sn atomic ratio equal to 3:1.

The presence of electronic and geometric effects in the bimetallic catalysts determined by several techniques (like XPS, H$_2$ chemisorption and benzene hydrogenation test reaction) plays a very important role in their behaviors for the methanol oxidation. It is the synergy of these effects that leads to a maximum catalytic activity for the methanol oxidation for the three PtSn catalysts prepared with a Pt:Sn atomic ratio equal to 3:1. On the contrary, at high Sn loadings, the

Table III. Onset potential of CO oxidation ($E_{CO,Onset}$) and electrochemical active surface (EAS) values of Pt/NT and Pt-Sn/NT catalysts.

Catalyst	$E_{CO,Onset}$ [mV vs Ag/AgCl]	EAS [m^2 g Pt^{-1}]
Polyol Method		
Pt/NT (EG)	365	29.39
Pt_5Sn_1/NT (EG)	132	31.03
Pt_3Sn_1/NT (EG)	119	40.96
Pt_1Sn_1/NT (EG)	172	40.00
Sodium Borohydride Reduction Method		
Pt/NT ($NaBH_4$)	479	12.06
Pt_5Sn_1/NT ($NaBH_4$)	145	9.49
Pt_3Sn_1/NT ($NaBH_4$)	115	8.85
Pt_1Sn_1/NT ($NaBH_4$)	118	5.90
Sodium Borohydride Reduction Method (in EG)		
Pt/NT ($NaBH_4$-EG)	241	10.39
Pt_5Sn_1/NT ($NaBH_4$-EG)	115	18.33
Pt_3Sn_1/NT ($NaBH_4$-EG)	115	12.02
Pt_1Sn_1/NT ($NaBH_4$-EG)	111	12.22

Table IV. Cyclic voltammetry results of Pt/NT and Pt-Sn/NT catalysts for methanol oxidation reaction.

Catalyst	Positive peak potential [mV vs Ag/AgCl]	Positive peak current [mA]	I_f/ I_b [-]
Polyol Method			
Pt/NT (EG)	760	10.23	1.22
Pt_5Sn_1/NT (EG)	706	8.76	1.22
Pt_3Sn_1/NT (EG)	729	12.44	1.18
Pt_1Sn_1/NT (EG)	705	9.75	0.97
Sodium Borohydride Reduction Method			
Pt/NT ($NaBH_4$)	713	2.78	1.15
Pt_5Sn_1/NT ($NaBH_4$)	699	3.48	1.14
Pt_3Sn_1/NT ($NaBH_4$)	709	6.20	1.11
Pt_1Sn_1/NT ($NaBH_4$)	670	2.63	1.05
Sodium Borohydride Reduction Method (in EG)			
Pt/NT ($NaBH_4$-EG)	706	1.93	1.14
Pt_5Sn_1/NT ($NaBH_4$-EG)	704	8.79	1.14
Pt_3Sn_1/NT ($NaBH_4$-EG)	701	8.88	1.13
Pt_1Sn_1/NT ($NaBH_4$-EG)	688	3.23	1.10
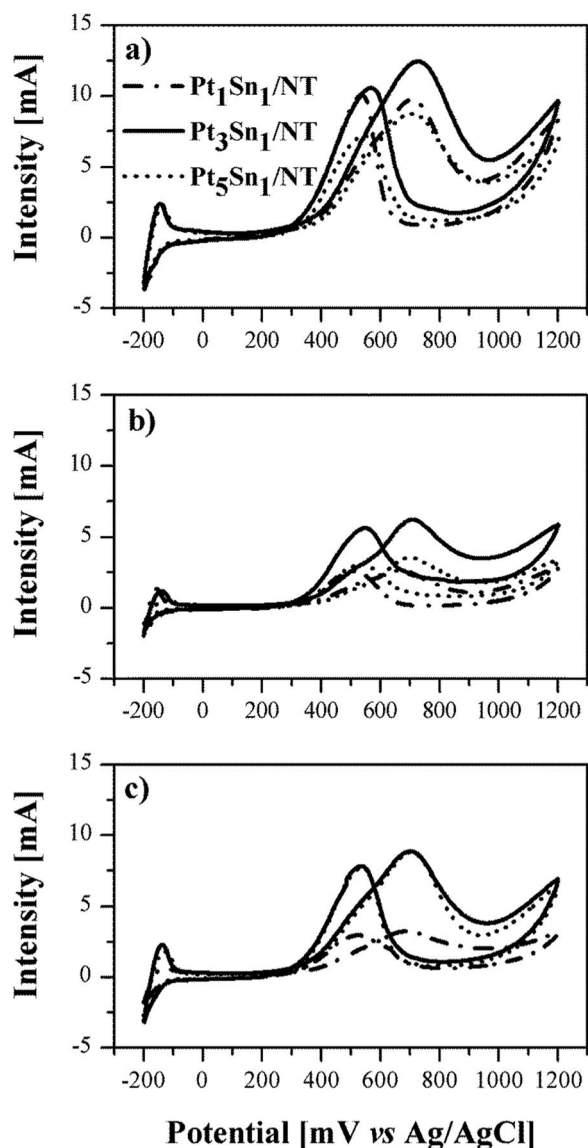
methanol oxidation activity sharply decreases, due to an important blocking effect of Sn on Pt sites.

On the other hand, Pt-Sn/NT ($NaBH_4$-EG) catalysts exhibit higher maximum current intensities by a factor of 1.2–2.5 (Table IV) compared to the corresponding Pt-Sn/NT ($NaBH_4$) catalyst, due to the stabilizing effect of ethylene glycolic $NaBH_4$ solution on Pt particles.

The Pt_3Sn_1/NT (EG) catalyst showed the best catalytic performance of all the prepared catalysts. The anodic current peak for methanol oxidation appears at 729 mV vs Ag/AgCl, and the current peak density is 12.44 mA cm^{-2} during positive potential scanning on this catalyst.

The ratio of the forward to reverse anodic current peak (I_f/I_b) can be used to evaluate the tolerance of the bimetallic catalysts to the accumulation of carbonaceous species.[56] In this sense, a low I_f/I_b ratio would be consistent with a low CO tolerance. I_f/I_b ratios are obtained from Figure 6 and shown in Table IV. As it is seen, the poison resistance ability has the following order: Pt_5Sn_1/NT $\geq Pt_3Sn_1$/NT > Pt_1Sn_1/NT for all the methods. This indicates that Pt_1Sn_1/NT catalysts (with the highest Sn contents) have the worst catalytic activities and are the most sensitive bimetallic catalysts to CO poisoning.

Among all the catalysts, the Pt_3Sn_1 sample prepared by EG displays the highest activity for methanol oxidation and has an adequate CO tolerance, this agreeing with the high electrochemical active surface (EAS) and H_2 chemisorption values displayed by this catalyst.

In order to test the behavior of Pt-Sn/NT catalysts in methanol oxidation, chronoamperometry measurements at 350 mV vs Ag/AgCl were carried out in solutions of 0.5 M H_2SO_4 + 1 M CH_3OH for 60 min. Figure 7 shows the curves of current intensity vs time. As it can be seen, there is an initial step in which the current quickly falls up to 5 min, then it gradually falls with time up to reach a constant value. These currents at high reaction times can characterize an equilibrium state of alcohol adsorption and oxidation. It can be seen that among all the catalysts Pt_3Sn_1/NT (EG) and Pt_3Sn_1/NT ($NaBH_4$-EG) ones are able to maintain the highest current density for over 1 h, thus reaching a similar current intensity (0.57 mA) in stationary state.

Figure 8 shows linear sweep voltammograms at 1 mV s^{-1} and 30°C for methanol oxidation, for mono and bimetallic catalysts. For potentials higher than 200 mV vs Ag/AgCl, Pt_3Sn_1/NT (EG) catalyst shows the higher activity for methanol oxidation as it gives higher oxidation current density than the other catalysts. On the other hand, the monometallic Pt catalysts display the lowest performance. The current densities increase in the following order: Pt/NT < Pt_1Sn_1/NT < Pt_5Sn_1/NT < Pt_3Sn_1/NT for EG, $NaBH_4$ and $NaBH_4$-EG methods.

Figure 6. Cyclic voltammograms for Pt-Sn/NT catalysts prepared by: a) EG; b) $NaBH_4$; and c) $NaBH_4$-EG methods. Electrolytic solution: 0.5 M H_2SO_4 + 1 M CH_3OH.
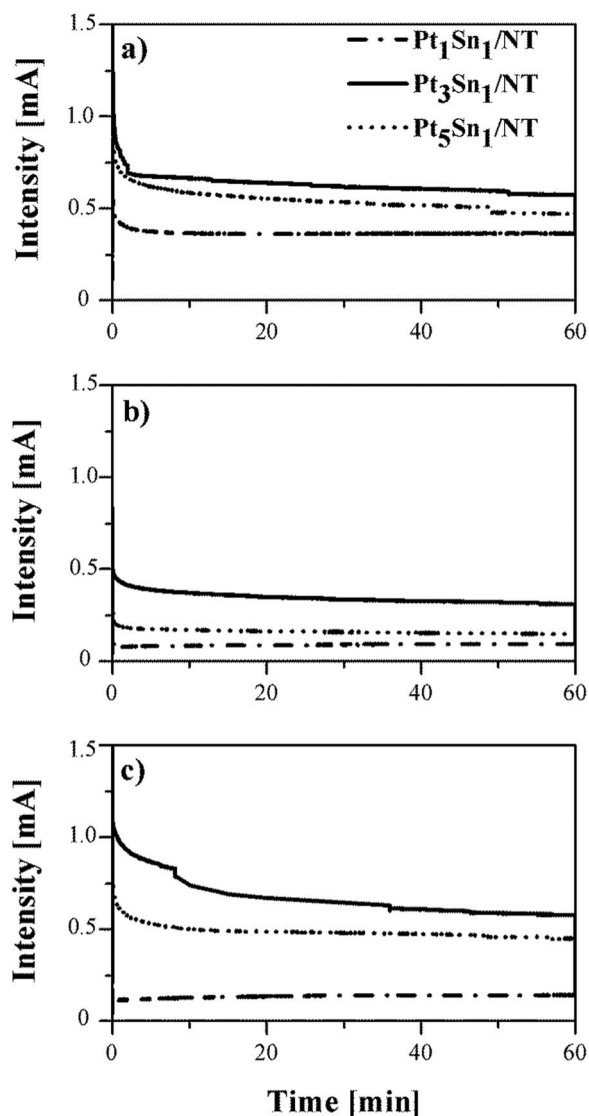
Figure 7. Chronoamperometry curves for Pt-Sn/NT catalysts prepared by: a) EG; b) NaBH$_4$; and c) NaBH$_4$-EG methods, recorded in 0.5 M H$_2$SO$_4$ + 1 M CH$_3$OH solution at 350 mV vs Ag/AgCl.

Figure 8. LSV voltammograms for Pt/NT and Pt-Sn/NT catalysts prepared by: a) EG; b) NaBH$_4$; and c) NaBH$_4$-EG methods. Electrolytic solution: 0.5 M H$_2$SO$_4$ + 1 M CH$_3$OH.

Conclusions

In the present study, multiwalled carbon nanotubes supported PtSn electrocatalysts with different Pt:Sn atomic ratios were easily prepared by two liquid phase reduction methods to be employed as anode material in low-temperature fuel cell.

Cyclic voltammetry measurements showed that the addition of Sn into the Pt catalyst promotes the activities for methanol electrooxidation, in which the maximum activities appeared at a Pt:Sn molar ratio equal to 3:1 for all the synthesis methods.

For sodium borohydride reduction method, a simple variation in the medium (EG instead of water) has been found to enhance the catalytic activity of Pt nanoparticles for MOR by 1.2–2.5 times. The ability of the Pt nanoparticles prepared by NaBH$_4$-EG to oxidize CO$_{ad}$ at a lower potential implies a favorable effect on MOR activity.

Among all the catalysts, the Pt$_3$Sn$_1$/NT sample prepared by EG displays the highest activity for methanol electrooxidation. Besides, this catalyst has a good CO tolerance and an important stability determined by chronoamperometry measurements. These results are in agreement with the very high electrochemical active surface and H$_2$ chemisorption values displayed by this catalyst, and also to a narrow distribution of metallic particles (determined by TEM).

References

1. J. C. Ho, E.-C. Saw, L. Y. Y. Lu, and J. S. Liu, *Technol. Forecast. Soc. Change*, **82**, 66 (2014).
2. K. Charoen, C. Prapainainar, P. Sureeyatanapas, T. Suwannaphisit, K. Wongamornpitak, P. Kongkachuichay, S. M. Holmes, and P. Prapainainar, *J. Clean. Prod.*, **142**, 1309 (2017).
3. R. Rizo, M. J. Lázaro, E. Pastor, and G. García, *Molecules*, **21**, 1225 (2016).
4. A. Dutta and J. Datta, *Int. J. Hydrogen Energy*, **38**, 7789 (2013).
5. E. Antolini, *ChemElectroChem*, **1**, 318 (2014).
6. L. A. Soares, C. Morais, T. W. Napporn, K. B. Kokoh, and P. Olivi, *J. Power Sources*, **315**, 47 (2016).
7. X. F. Jiang, X. B. Wang, L. M. Shen, Q. Wu, Y. N. Wang, Y. W. Ma, X. Z. Wang, and Z. Hu, *Chin. J. Catal.*, **37**, 1149 (2016).
8. G. F. Long, X. H. Li, K. Wan, Z. X. Liang, J. H. Piao, and P. Tsiakaras, *Appl. Catal. B-Environ.*, **203**, 541 (2017).
9. E. Antolini, *Appl. Catal. B: Environ.*, **74**, 337 (2007).

10. M. Carmo, M. Brandalise, A. Oliveira Neto, E. V. Spinacé, A. D. Taylor, M. Linardi, and J. R. G. Poco, *Int. J. Hydrogen Energy*, **36**, 146592 (2011).
11. M. D. Mobarakeh, *Fiber. Polym.*, **18**, 95 (2017).
12. E. Antolini, F. Colmati, and E. R. Gonzalez, *J. Power Sources*, **193**, 555 (2009).
13. N. S. Veizaga, V. I. Rodriguez, T. A. Rocha, M. Bruno, O. A. Scelza, S. R. de Miguel, and E. R. Gonzalez, *J. Electrochem. Soc.*, **162**, F243 (2015).
14. R. G. C. S. dos Reis and F. Colmati, *J. Solid State Electrochem.*, **20**, 2559 (2016).
15. O. Ugalde-Reyes, R. Hernández-Maya, A. L. Ocampo-Flores, F. Alvarez-Ramírez, E. Sosa-Hernández, C. Angeles-Chavez, and P. Roquero, *J. Electrochem. Soc.*, **162**, H132 (2015).
16. C.-T. Hung, Z.-H. Liou, P. Veerakumar, P.-H. Wu, T.-C. Liu, and S.-B. Liu, *Chinese J. Catal.*, **37**, 43 (2016).
17. Z. Ji, X. Shen, G. Zhu, K. Chen, G. Fu, and L. Tong, *J. Electroanal. Chem.*, **682**, 95 (2012).
18. A. Hassan, V. A. Paganin, and E. A. Ticianelli, *J. Power Sources*, **325**, 375 (2016).
19. E. V. Spinacé, R. R. Dias, M. Brandalise, M. Linardi, and A. Oliveira Neto, *Ionics*, **16**, 91 (2010).
20. F. E. López-Suárez, M. Perez-Cadenas, A. Bueno-López, C. T. Carvalho-Filho, K. I. B. Eguiluz, and G. R Salazar-Banda, *J. Appl. Electrochem.*, **45**, 1057 (2015).
21. M. K. Jeon and P. J. McGinn, *J. Power Sources*, **194**, 737 (2009).
22. L. Dong, H. Dong, L. Yu, Q. Zhang, J. Bai, J. Sui, and B. Ma, *ECS Trans.*, **41**, 1317 (2011).
23. F. Colmati, E. Antolini, and E. R. Gonzalez, *Electrochim. Acta*, **50**, 5496 (2005).
24. E. Antolini and E. R. Gonzalez, *Electrochim. Acta*, **56**, 1 (2010).
25. E. Antolini and E. R. Gonzalez, *Catal. Today*, **160**, 28 (2011).
26. I. Borbath, D. Guban, Z. Paszti, I. E. Sajo, E. Drotar, J. L. Gomez de la Fuente, T. Herranz, S. Rojas, and A. Tompos, *Top. Catal.*, **56**, 1033 (2013).
27. A. S. Aricò, D. Sebastian, S. C. Zignani, and V. Baglio, *ECS Trans.*, **69**, 833 (2015).
28. F. Vigier, C. Coutanceau, A. Perrard, E. M. Belgsir, and C. Lamy, *J. Appl. Electrochem.*, **34**, 439 (2004).
29. D. Wanga, S. Lu, and S. P. Jiang, *Electrochim. Acta*, **55**, 2964 (2010).
30. P. E. Tsiakaras, *J. Power Sources*, **171**, 107 (2007).
31. O. V. Korchagin, V. T. Novikov, E. G. Rakov, V. V. Kuznetsov, and M. R. Tarasevich, *Russ. J. Electrochem.*, **46**, 882 (2010).
32. B. Liu, Z.-W. Chia, Z.-Y. Lee, C.-H. Cheng, J.-Y. Lee, and Z.-L. Liu, *Fuel Cells*, **12**, 670 (2012).
33. D. M. Han, Z. P. Guo, R. Zeng, C. J. Kim, Y. Z. Meng, and H. K. Liu, *Int. J. Hydrogen Energy*, **34**, 2426 (2009).
34. C.-T. Hsieh, Y.-S. Chang, and K.-M. Yin, *J. Phys. Chem. C*, **117**, 15478 (2013).
35. M. P. Pechini, Pat. number 3.330.697, USA, 1967.
36. J. Ribeiro, D. M. dos Anjos, K. B. Kokoh, C. Coutanceau, J.-M. Leger, P. Olivi, A. R. de Andrade, and G. Tremiliosi-Filho, *Electrochim. Acta*, **52**, 6997 (2007).
37. F. L. S. Purgato, S. Proniera, P. Olivi, A. R. de Andrade, J. M. Léger, G. Tremiliosi-Filho, and K. B. Kokoh, *J. Power Sources*, **198**, 95 (2012).
38. A. Bonesi, M. Asteazaran, M. S. Moreno, G. Zampieri, S. Bengio, W. Triaca, and A. M. Castro Luna, *J. Solid State Electrochem.*, **17**, 1823 (2013).
39. L. Jiang, H. Zang, G. Sun, and Q. Xin, *Chin. J. Catal.*, **27**, 15 (2006).
40. J. J. Linares, T. A. Rocha, S. Zignani, V. A. Paganin, and E. R. Gonzalez, *Int. J. Hydrogen Energy*, **38**, 620 (2013).
41. G. C. Torres, E. L. Jablonski, G. T. Baronetti, A. A. Castro, S. R. de Miguel, O. A. Scelza, M. D. Blanco, M. A. Peña Jimenez, and J. L. G. Fierro, *App. Cat. A Gen.*, **161**, 213 (1997).
42. I. M. J. Vilella, S. R. de Miguel, C. Salinas-Martínez de Lecea, Á. Linares-Solano, and O. A. Scelza, *Appl. Cat. A Gen.*, **281**, 247 (2005).
43. S. Q. Song, W. J. Zhou, Z. H. Zhou, L. H. Jiang, G. Q. Sun, Q. Xin, V. Leontidis, S. Kontou, and P. Tsiakaras, *Int. J. Hydrogen Energy*, **30**, 995 (2005).
44. D. Chu, Z. Li, X. Yuan, J. Li, X. Wei, and Y. Wan, *Electrochim. Acta*, **78**, 644 (2012).
45. J. B. Joo, P. Kim, W. Kim, Y. Kim, and J. Yi, *J. Appl. Electrochem.*, **39**, 135 (2009).
46. F. Maillard, M. Eikerling, O. V. Cherstiouk, S. Schreier, E. Savinova, and U. Stimming, *Faraday Discuss*, **125**, 357 (2004).
47. N. Veizaga, J. Fernandez, M. Bruno, O. Scelza, and S. de Miguel, *Int. J. Hydrogen Energy*, **37**, 17910 (2012).
48. S. R. de Miguel, O. A. Scelza, M. C. Roman-Martinez, C. Salinas-Martinez de Lecea, D. Cazorla-Amoros, and A. Linares-Solano, *Appl. Catal. A Gen.*, **170**, 93 (1998).
49. C. D. Wagner, W. M. Riggs, L. E. Davis, J. F. Moulder, and G. E. Muilenberg, *Handbook of X-ray photoelectron spectroscopy*, Perkin- Elmer CO: Physical Electronics, 1979.
50. D. Poondi and M. A. Vannice, *J. Catal.*, **161**, 742 (1996).
51. G. L. Haller, *J. Catal.*, **216**, 12 (2003).
52. E. Lee, A. Murthy, and A. Manthiram, *Electrochem. Comm.*, **13**, 480 (2011).
53. T. Vidakovic, M. Christov, and K. Sundamcher, *Electrochim. Acta*, **52**, 5606 (2007).
54. N. Veizaga, V. Paganin, T. Rocha, O. Scelza, S. de Miguel, and E. Gonzalez, *Int. J. Hydrogen Energy*, **39**, 8728 (2014).
55. N. M. Markovic and P. N. Ross, *Surf. Sci. Rep.*, **45**, 121 (2002).
56. Z. L. Liu, X. Y. Ling, X. D. Su, and J. Yang, *J. Phys. Chem. B*, **108**, 8234 (2004).